Phosphorylation of Aquaporin PvTIP3;1 Defined by Mass Spectrometry and Molecular Modeling†

Mark J. Daniels‡ and Mark Yeager*,‡,§

Department of Cell Biology, The Scripps Research Institute, 10550 North Torrey Pines Road, La Jolla, California 92037, and Division of Cardiovascular Diseases, Scripps Clinic, 10666 North Torrey Pines Road, La Jolla, California 92037

Received March 28, 2005; Revised Manuscript Received August 16, 2005

ABSTRACT: The water channel protein PvTIP3;1 (α-TIP) is a member of the Major Intrinsic Protein membrane channel family. The in vitro activity of this aquaporin is dependent on phosphorylation, and the protein is phosphorylated in vivo by a membrane-associated Ca^{2+}-dependent kinase. Mutagenesis studies have implicated three serine residues as kinase targets, but only phosphorylation of Ser7 has been observed in vivo. An atomic model of PvTIP3;1 generated by homology modeling suggested that Ser7 is the only residue that would be sterically accessible to kinases. To further explain the phosphorylation of PvTIP3;1, we overexpressed this aquaporin in the methylotrophic yeast *Pichia pastoris* and purified the hexahistidine-tagged protein by immobilized metal affinity chromatography. Mass spectrometry confirmed that a fraction of recombinant PvTIP3;1 was phosphorylated. Phosphatase and kinase treatments indicated that Ser7 was the only residue that could be phosphorylated. In addition, mass spectrometry indicated that the native and expressed proteins are N-terminally acetylated. This is the first demonstration that a full-length, recombinant aquaporin can be produced in yeast and authentically phosphorylated in vitro. Characterization of phosphorylation-mediated gating in PvTIP3;1 will serve as a paradigm for understanding gating mechanisms of other channels.

The first water channel was cloned serendipitously during the characterization of human blood group antigens and was found to encode a putative channel in the red blood cell plasma membrane (*1*). By expressing the protein in *Xenopus* toad oocytes, its function as a water channel was suggested by a concomitant increase in the swelling rate of osmotically shocked cells (*2*). This demonstration of water channel activity ended decades of speculation that proteins were responsible for the high water permeability observed in certain biological membranes.

Over the last decade, many organisms have been shown to possess a class of protein channels, termed "aquaporins", which are specialized to facilitate the transcellular movement of water. Aquaporins are members of the Major Intrinsic Protein (MIP)[1] superfamily, found in animals, plants, insects, and bacteria (*3*−*6*). Generally, aquaporins facilitate the movement of water across cell membranes in response to osmotic gradients, functioning in cellular and organismal osmoregulation and solute transport (*7*−*9*).

Recent high-resolution structures derived by electron and X-ray crystallography suggest that selectivity for water is accomplished by a filter that excludes larger molecules and a hydrophobic entrance to the pore that blocks the passage of hydrated ions (*10*−*12*). Electrostatic interactions between highly conserved asparagine residues and water molecules in the pore disrupt the hydrogen bonding pattern that would be formed by the chain of water molecules, thereby preventing the conduction of protons (*11*). The unusual combination of a hydrophobic pore and a small number of solute binding sites was proposed to facilitate water transport (*12*).

PvTIP3;1 (formerly named α-TIP) is a plant aquaporin found in bean seed vacuole membranes (*13*). In a *Xenopus* oocyte water channel assay (*2*), PvTIP3;1 shows weak water channel activity (*14*) that is greatly increased when the oocytes are treated with kinase-activating and phosphatase-inhibiting compounds (*14*). The protein undergoes phosphorylation in vivo during seed germination by a membrane-associated, calcium-dependent protein kinase (CDPK) (*15*) and can also be phosphorylated in vitro by plant and animal kinases (*14*). Phosphorylation increases the water channel activity of PvTIP3;1 expressed in *Xenopus* oocytes (*14*). It may therefore be inferred that PvTIP3;1 phosphorylation enhances the rehydration of the protein storage vacuole, thereby facilitating the enzymatic breakdown of stored compounds and the release of nutrients (*13*). Ser7 at the amino-terminus is phosphorylated in vivo upon germination (*15*); however, phosphorylation at Ser23 and Ser99 may also participate in PvTIP3;1 regulation (*14*).

Phosphorylation of water channels may be a widespread mechanism for regulating transmembrane water flux in

† M.J.D. was supported by an NIH NRSA fellowship (EY06906). M.Y. was supported by grants from the NIH, NHLBI (R01 HL48908), and NIGMS (R01 GM65399). During this work, M.Y. was a recipient of a Clinical Scientist Award in Translational Research from the Burroughs Wellcome Fund.

* To whom correspondence should be addressed. E-mail: yeager@scripps.edu. Phone: (858) 784-8584. Fax: (858) 784-2504.

‡ The Scripps Research Institute.

§ Scripps Clinic.

[1] Abbreviations: MIP, major intrinsic protein; CDPK, calcium-dependent protein kinase; MALDI-TOF MS, matrix-assisted laser desorption ionization time-of-flight mass spectrometry; TEA, triethanolamine; MES, 2-(*N*-morpholino)ethanesulfonate; DTT, dithiothreitol; DeS, *n*-decanoylsucrose; TFA, trifluoroacetic acid; λ-PPase, phage λ protein phosphatase; PKA, protein kinase A.

10.1021/bi050565d CCC: $30.25
Published on Web 10/11/2005

plants. The plant aquaporin SoPIP2;1 (PM28a) is regulated by phosphorylation via a membrane-associated CDPK (*16*). The protein is dephosphorylated as a result of lowered extracellular (apoplastic) water potential, suggesting that water transport activity is reduced during increased water stress (*17*). These results suggest a role for SoPIP2;1 in the drought stress response in which water stress leads to closure of SoPIP2;1 water channels and a reduction in water loss from the cell (*17*, *18*). GmNod26, found in the soybean symbiosome membrane of root nodules, is also phosphorylated at its C-terminus by a membrane-associated CDPK (*19*), which results in enhanced water permeability (*20*). Phosphorylation occurs during root nodule organogenesis and following osmotic stress (*20*). Phosphorylation in vitro, by a Mg^{2+}-dependent protein kinase, has also been observed with PvTIP3;1 homologues from lentil seed (*21*).

The mechanism of PvTIP3;1 aquaporin regulation by phosphorylation is unknown, even though a number of plant aquaporins appear to share this ability. In contrast, mammalian aquaporins are typically in a constitutively open conformation and regulation is achieved by modulating protein abundance through vesicle-mediated transport of the channels to the plasma membrane (*22*). To investigate the phosphorylation-dependent activity of water channels, we developed an overexpression system in *Pichia pastoris*. Recombinant PvTIP3;1 can be appropriately phosphorylated and dephosphorylated in vitro by protein kinase A (PKA) at Ser7, as determined by matrix-assisted laser desorption ionization time-of-flight mass spectrometry (MALDI-TOF MS). A molecular model of PvTIP3;1 was generated by homology modeling, from which it can be inferred that Ser7 is the only residue accessible to serine kinases.

EXPERIMENTAL PROCEDURES

Construction and Overexpression of PvTIP3;1-G_3-H_6 in P. pastoris. The sequence flanking the *Phaseolus vulgaris* PvTIP3;1 aquaporin cDNA (*23*) was modified by PCR to facilitate cloning and protein purification. Two oligonucleotide primers were constructed for this purpose. The forward strand primer was 5′-CGAG GAATTC ATG GCT ACC CGA AGA TAT TCT TTT GGA AG-3′, which incorporates an EcoRI restriction site before the *PvTIP3;1* start codon. This sequence also introduced a conservative base pair change in the second codon (GCA to GCT) that created an Ala codon preferred by yeast (*24*). The reverse strand primer was 5′-TGT TCTAGA TCA ATG GTG ATG GTG ATG GTG CCC ACC CCC GTA ATC TTC AGT TGC CAA AGG-3′, which added an amino-terminal G_3-H_6 tag before the *PvTIP3;1* stop codon and introduced an XbaI restriction site. PCR was performed using Deep Vent DNA polymerase (New England Biolabs). The resulting PCR fragment was cut with EcoRI and XbaI, purified by electrophoresis in an agarose gel, and extracted from the agarose using a gel extraction kit (Qiagen). This PvTIP3;1 gene fragment was subcloned into the *P. pastoris* expression vector PICZ-B (Invitrogen) that was cut with EcoRI and XbaI, purified by electrophoresis in an agarose gel, and extracted from the agarose using a gel extraction kit (Qiagen). PvTIP3;1 and PICZ-B were ligated together using T4 DNA ligase (New England Biolabs). This *PvTIP3;1-G_3-H_6*/pPICZ construct was transformed into *Escherichia coli* strain XL1-Blue (Stratagene). Transformants were selected by plating on low-salt LB agar containing the antibiotic zeocin at a concentration of 25 μg/mL. Plasmid DNA was isolated using a plasmid purification kit (Qiagen), and the fidelity of *PvTIP3;1-G_3-H_6* was verified by DNA sequencing. Prior to yeast transformation by homologous recombination, the *PvTIP3;1-G_3-H_6*/pPICZ plasmid was linearized with BstXI. Transformation of *P. pastoris* yeast strain KM71H with the linearized plasmid was carried out using the *Pichia* EasyComp kit (Invitrogen). Transformants were selected by plating the treated yeast on YPDS agar containing the antibiotic zeocin at a concentration of 100 μg/mL. Preparation of PvTIP3;1-overexpressing *P. pastoris* was started by culturing an isolated yeast colony in 10 mL of BMGY medium [1% yeast extract, 2% peptone, 1.34% yeast nitrogen base, 100 mM potassium phosphate (pH 6.0), 4×10^{-5} % biotin, and 1% glycerol] overnight at 30 °C with shaking at 275 rpm. A larger volume of BMGY medium (100 mL to 1 L) was inoculated with a 1/100 volume of the starting culture. The second culture was incubated for approximately 12 h at 30 °C with shaking at 275 rpm. Cells were harvested at an OD_{600nm} between 1 and 4 and pelleted by centrifugation for 5 min at 1500*g*. Induction of protein expression was initiated by resuspending the yeast cells in BMMY medium [1% yeast extract, 2% peptone, 1.34% yeast nitrogen base, 100 mM potassium phosphate (pH 6.0), 4×10^{-5} % biotin, and 1% methanol] to an OD_{600nm} of 0.5−2. Incubation was continued at 30 °C with shaking at 250 rpm for baffled culture flasks or 300 rpm for unbaffled culture flasks. A supplemental volume of methanol equal to 1/100 of the culture volume was added every 16 h. Following induction for 24−40 h, the culture was chilled on ice and stored at 4 °C.

Purification of PvTIP3;1-G_3-H_6. Cells from a culture of induced, PvTIP3;1-G_3-H_6-overexpressing *P. pastoris* were harvested by centrifugation for 5 min at 1500*g*. The cell pellet was frozen and stored at −80 °C. To prepare spheroplasts, cells were thawed at 4 °C and resuspended in Spheroplasting Buffer [1.5 M sorbitol, 50 mM triethanolamine (TEA) (pH 7.5), 10 mM sodium azide, and 10 mM benzamidine], in a volume of 2 mL/g of pelleted cells. β-Mercaptoethanol was added to a final concentration of 30 mM, followed by addition of yeast lytic enzyme (ICN Biomedicals) at a concentration of 400 units of lytic activity/g of cell pellet. This cell suspension was then incubated at 30 °C for 1 h with gentle, magnetic stirring. Yeast spheroplasts were harvested by centrifugation for 5 min at 2000*g*. Subsequent steps were carried out at 4 °C or on ice. The cell pellet was washed by resuspension in cold Spheroplasting Buffer and isolated by centrifugation for 5 min at 5000*g*. Pelleted spheroplasts were frozen at −80 °C, thawed, and resuspended in Lysis Buffer [50 mM TEA (pH 7.5), 10 mM benzamidine, 5 mM EDTA, 5 mM EGTA, 1 mM 1,10-phenanthroline, 1 mM dithiothreitol (DTT), 10 μM leupeptin, 5 μM pepstatin A, and 1 μM aprotinin], in a volume of 3 mL/g of spheroplast pellet. Cells were stirred and lysed by sonication with fifteen 30 s, 20 kHz bursts at a power of 75 W using a microtip probe (Misonix part 420). Each sonication burst was followed by a 1 min cooling interval on ice. Phenylmethanesulfonyl fluoride in dimethyl sulfoxide was added to a final concentration of 1 mM immediately before the start of sonication. Cell debris was removed by centrifugation for 10 min at 2000*g* and 4 °C. Yeast microsomes were then harvested by centrifugation for 1 h at 25000*g* and 4 °C.

Membrane protein solubilization and nickel affinity chromatography were adapted from the procedures of Jahn et al. (*25*). The microsomal pellet was resuspended in cold Solubilization Buffer [50 mM 2-(*N*-morpholino)ethanesulfonate (MES) (pH 6.5), 20% glycerol (v/v), and 2 mM β-mercaptoethanol] in a volume of 20 mL/g of microsomal pellet. This suspension was stirred at 4 °C, and dry *n*-decanoylsucrose (DeS) was slowly added, up to a quantity equal to half of the microsomal pellet mass, which produced a solution of ~2.5% (w/v) detergent. Microsomes were then stirred for 2.5 h at 4 °C, and then insoluble material was removed by centrifugation for 1 h at 100000*g* and 4 °C. The supernatant was diluted with an equal volume of Binding Buffer [50 mM MES (pH 6.5), 500 mM NaCl, 20% glycerol, 50 mM imidazole, and 0.2% DeS (w/v)]. Ni−NTA Superflow resin (Pharmacia) was then added in a volume of 250 μL of packed resin per gram of microsome pellet. Prior to use, the Ni−NTA Superflow resin was washed twice with water and once with Binding Buffer. Solubilized microsomes and resin were mixed together by gentle stirring for 20 h at 4 °C. The suspension was poured into an 0.8 cm × 4 cm plastic chromatography column (Bio-Rad), and the liquid was drained. Collected resin was washed twice with 10 column volumes of Washing Buffer [50 mM MES (pH 6.5), 250 mM NaCl, 20% glycerol (v/v), 50 mM imidazole, and 0.2% DeS (w/v)]. The resin was then washed with 10 column volumes of Equilibration Buffer [50 mM TEA (pH 7.5), 100 mM NaCl, 20% glycerol (v/v), 50 mM imidazole, and 0.2% DeS (w/v)]. Bound protein was eluted by washing the column resin with 4 column volumes of Elution Buffer [50 mM TEA (pH 7.5), 20% glycerol (v/v), 500 mM imidazole, 100 mM NaCl, 1 mM DTT, and 0.25% DeS (w/v)]. The eluted protein was concentrated using Centricon-50 centrifugal filter devices (Amicon), which had been previously treated for 10 min with Equilibration Buffer. Buffer exchange was performed by diluting the concentrated protein in Storage Buffer [50 mM TEA (pH 7.5), 100 mM NaCl, 0.25% DeS (w/v), 3 mM sodium azide, and 1 mM DTT] and reconcentrating the sample by centrifugal filtration as described above. SDS−PAGE chromatography and Western immunoblotting were performed as previously described (*26*).

In Vitro Phosphorylation and Dephosphorylation of PvTIP3;1. For phosphorylation, 3 μg of Ni−NTA-purified PvTIP3;1 was incubated for 2 h at room temperature in a solution of 25 mM NH_4HCO_3 (pH 7.4), 5 mM DeS, 5 mM $MgCl_2$, 2 mM DTT, 5 mM ATP, and 25 units of bovine PKA catalytic subunit (Sigma). For dephosphorylation, 3 μg of Ni−NTA-purified PvTIP3;1 was incubated for 2 h at room temperature in a solution of 25 mM NH_4HCO_3, 5 mM DeS, 5 mM $MnCl_2$, 2 mM DTT, and 250 units of λ protein phosphatase (New England Biolabs).

CNBr Digestion and Mass Spectrometry. Native PvTIP3;1 was prepared from dry *Ph. vulgaris* seed as previously described (*26*). Either native PvTIP3;1 or *Pichia*-expressed PvTIP3;1-G_3-H_6 was denatured by heating for 30 min at 37 °C in 2% SDS, 20 mM Tris-HCl (pH 6.8), 10% glycerol, and 100 mM DTT. SDS−PAGE chromatography was performed as previously described (*26*), and the gel-bound protein was electroblotted onto a nitrocellulose membrane (Schleicher & Schuell Protran BA83) for 2 h at 100 V in 20% methanol, 25 mM Tris-HCl (pH 8), 192 mM glycine, and 0.01% SDS. Ponceau S stain was used to visualize the band corresponding to PvTIP3;1, which was excised using a clean scalpel. The excised nitrocellulose strip (~7 mm^2) was washed three times for 10 s with 200 μL of water and then dried under vacuum. Bound PvTIP3;1 was proteolytically cleaved by immersing the strip in an aqueous solution of 0.5 M CNBr, 0.1 N HCl, and 10% acetonitrile for 12−24 h at 22 °C under argon in the dark. The nitrocellulose was then washed once with water and dried under vacuum. Prior to MALDI-TOF MS, the nitrocellulose strip was dissolved in 15 μL of 96% acetone and 4% trifluoroacetic acid. Aliquots (0.2 μL) of the cleared solution were spotted onto a stainless steel sample plate. The spot was resuspended in 1.5 μL of 96% acetone, 3% trifluoroacetic acid, and 1% water with α-cyanohydroxycinnamic acid at 15 mg/mL, and then allowed to dry. Sample spotting, matrix addition, and drying were performed at 4 °C. MALDI-TOF mass spectra were recorded with a PerSeptive Biosystems Voyager-DE mass spectrometer with delayed extraction and TOF mass analyzer. Bradykinin fragment 1-7 and bovine erythocyte ubiquitin were used as external standards for mass calibration.

Trypsin Digestion and Mass Spectrometry. Native PvTIP3;1 was prepared from dry *Ph. vulgaris* seed as previously described (*26*). Aliquots of recombinant TIP3;1-G_3-H_6 were diluted in PFOA Buffer (25 mM NH_4HCO_3 and 6 mM pentadecafluorooctanoic acid) and then concentrated using Microcon-100 centrifugal filter devices (Amicon), which had been previously treated for 10 min with PFOA Buffer. Buffer exchange was performed by diluting the concentrated protein in PFOA Buffer and reconcentrating the sample by centrifugal filtration as described above. Sequencing-grade trypsin (Promega) was added in a quantity of 0.2 μg of trypsin per 10 μg of protein, and proteolysis was performed for 12 h at 37 °C. The resulting peptide solution was concentrated in a centrifugal evaporator. Aliquots (0.5 μL) of the concentrated solution were spotted onto a stainless steel sample plate. The spot was mixed with 0.5 μL of 60% acetonitrile (v/v) and 1% trifluoroacetic acid in water with α-cyanohydroxycinnamic acid at 10 mg/mL and then allowed to dry. Sample spotting, matrix addition, and drying were performed at room temperature. MALDI-TOF mass spectra were recorded with a PerSeptive Biosystems Voyager-DE mass spectrometer with delayed extraction and TOF mass analyzer. Bradykinin fragment 1-8 and the α-cyanohydroxycinnamic acid matrix dimer were used as external standards for mass calibration.

In-gel trypsin digestion of native PvTIP3;1 samples was performed as previously described (*27*). MALDI-TOF mass spectra were recorded with a PerSeptive Biosystems Voyager-STR mass spectrometer with delayed extraction and TOF reflectron mass analyzer.

Molecular Modeling. Amino acid sequences corresponding to human AQP1, bovine AQP1, and ovine AQP0 (GenBank accession numbers P29972, P47865, and AY573927, respectively) were aligned with PvTIP3;1 using the T-Coffee method (*28*), with manual adjustments to move gaps out of transmembrane α-helical domains. This alignment was used in conjunction with the associated structure files (Protein Data Bank entries 1H6I for human AQP1, 1J4N for bovine AQP1, and 1SOR for ovine AQP0) to generate molecular models using the Modeller software package [release 6v2 (*29*)]. A set of five possible models was produced, with a single "very-fast" thermal annealing step and 50 cycles of conjugate gradient energy minimization applied to each.

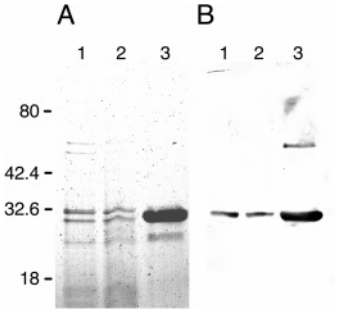

FIGURE 1: Purification of recombinant PvTIP3;1-G_3-H_6. (A) Coomassie-stained gel. (B) Western immunoblots of the equivalent gel, prepared with PvTIP3;1 antiserum (*46*): lane 1, *n*-decanoylsucrose-solubilized *P. pastoris* membranes; lane 2, solubilized membrane material not chelated by immobilized Ni^{2+}; and lane 3, solubilized membrane material chelated by Ni^{2+} and released by imidazole. Positions of molecular mass markers are indicated on the side with the respective mass in kilodaltons. The band at ~60 kDa in lane 3 of panel B is a dimer of PvTIP3;1-G_3-H_6.

Simulated thermal annealing was performed within the Modeller package, and conjugate gradient energy minimization was performed using the CNS software suite (*30*). Model stereochemistry was evaluated using Procheck (*31*). Structural alignments and comparisons were carried out using the TOPP routine in the CCP4 software package (*32*). Molecular graphics images were produced using UCSF-Chimera software (*33*). Disorder-based predictions of protein phosphorylation sites were performed using DISPHOS [version 1.3 (*34*)]. Predictions were calculated using both plant (*Arabidopsis thaliana*) and yeast (*Saccharomyces cerevisiae*) proteome membrane protein training sets.

RESULTS

Purification of Overexpressed PvTIP3;1-G_3-H_6. The methylotrophic yeast *P. pastoris* is increasingly being used as a protein expression system (*35*). The PvTIP3;1 gene was subcloned into the pPICZ *P. pastoris* expression vector (*36*) and modified to include a carboxy-terminal extension of three glycine and six histidine residues to facilitate purification by immobilized nickel affinity chromatography. The final gene construct (*PvTIP3;1-G_3-H_6*) was linearized and integrated into the yeast genome by homologous recombination, and recombinant yeast cells were selected by antibiotic screening. Since gene expression was under the control of the *AOX1* alcohol oxidase promoter, protein production was induced by switching to methanol as the sole carbon source in the growth medium. The growth rate of yeast expressing the recombinant protein was ~35% of the wild-type rate (data not shown).

Following induction of protein expression, yeast cells were harvested by centrifugation and lysed to isolate the membrane fraction. Sonication, French press, or yeast lytic enzyme treatment alone was inefficient in lysing PvTIP3;1-expressing *P. pastoris* (results not shown). Improved disruption of induced *P. pastoris* cells required a series of lytic treatments. Exposure to yeast lytic enzyme followed by sonication in hypo-osmotic media produced the most reproducible and efficient cell breakage. Cell debris was removed by low-speed centrifugation, and yeast membranes were then harvested by high-speed centrifugation. The resulting membrane pellet was solubilized with the nonionic detergent

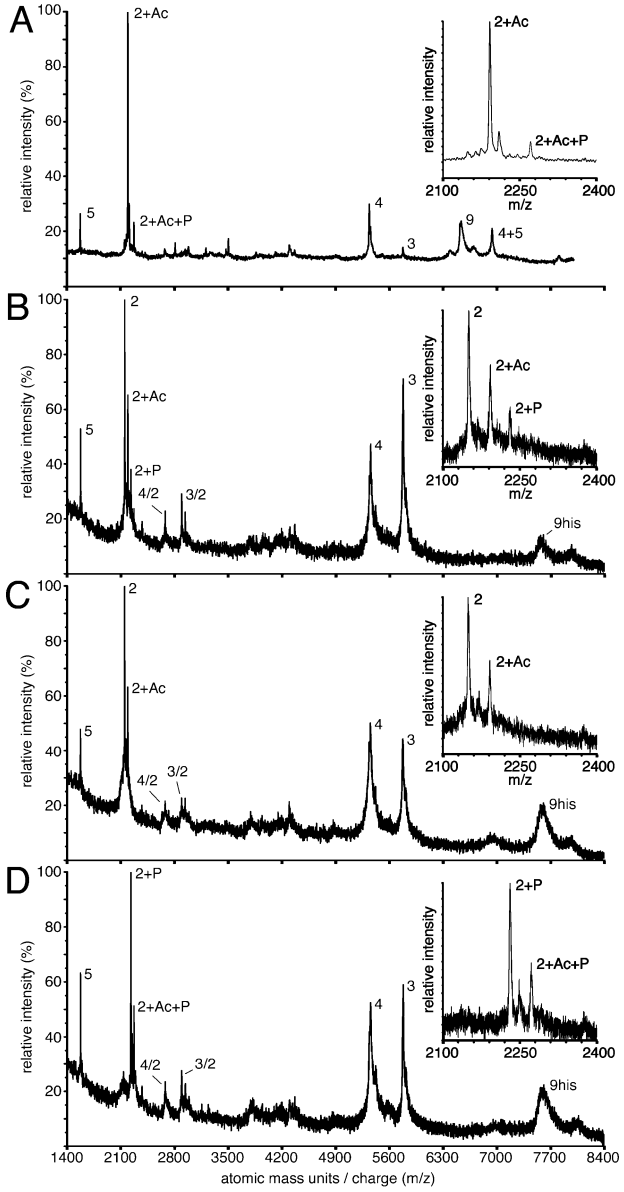

FIGURE 2: Linear MALDI-TOF mass spectra from CNBr digests of native PvTIP3;1 from *Ph. vulgaris* and PvTIP3;1-G_3-H_6 expressed in *P. pastoris*. Peaks labeled by fragment number as described in Table 1. Ac denotes peptide acetylation, and the letter P denotes peptide phosphorylation. The inset in each panel shows expanded spectra of fragment 2. (A) Native PvTIP3;1. The fragment 2 peak is followed by minor peaks at *m*/*z* +18 (homoserine derivative resulting from CNBr digestion) and *m*/*z* +80 (peptide phosphorylation). (B) Recombinant PvTIP3;1-G_3-H_6 expressed in *Pichia*. The fragment 2 peak is followed by minor peaks at *m*/*z* +42 (peptide acetylation) and *m*/*z* +80 (peptide phosphorylation). (C) Recombinant PvTIP3;1-G_3-H_6 treated with λ-PPase. The fragment 2 peak is followed by a minor peak at *m*/*z* +42 (peptide acetylation); the second peak of the phosphorylated peptide is no longer evident. (D) Recombinant PvTIP3;1-G_3-H_6 treated with PKA. The fragment 2 peak is not present; the major peak is from the phosphorylated peptide at *m*/*z* +80, followed by a minor peak at *m*/*z* +122 for a peptide that is both acetylated and phosphorylated. A peak from the homoserine derivative is also present. Note that peaks of other PvTIP3;1-G_3-H_6 fragments do not experience significant changes in mass with either λ-PPase or PKA treatment, suggesting that no other cytoplasmic serine residues are phosphorylated.

n-decanoylsucrose (DeS). One-step purification of PvTIP3;1-G_3-H_6 was accomplished using the affinity of the C-terminal hexahistidine for gel bead-immobilized Ni^{2+}.

Table 1: Predicted and Observed Cyanogen Bromide Fragments of PvTIP3;1[a]

			Observed mass			
			PvTIP3;1-G_3-H_6 expressed in *Pichia pastoris*			Native PvTIP3;1
			treatment			
Fragment	Residues	Expected mass	Untreated	PKA	λ-PPase	Untreated
1	1	102.1	-	-	-	-
2	2-20	2151.3	2151, +42, +80	2231, +42	2150, +42	2192, +80
3	21-77	5781.6	5780	5781	5780	5773
4	78-128	5342.3	5358	5361	5353	5335
5	129-144	1573.8	1573	1573	1573	1573
4+5	78-144	6945.2	-	-	-	6934
6	145-151	803.0	-	-	-	-
7	152-156	520.6	-	-	-	-
8	157-198	4129.8	-	-	-	-
9	199-256	6524.5				6531
9his	199-265	7518.5	7535	7602	7595	

Fragment	Amino Acids
1	M
2	ATRRY**S**FGRTDEATHPDSM
3	RA**S**LAEFASTFIFVFAGEGSGLALVKIYQDSAFSAGELLALALAHAFALFAAVSASM
4	HVSGGHVNPAVTFGALIGGRI**S**VIRAVYYWIAQLLGSIVAALVLRLVTNNM
5	RPSGFHVSPGVGVGHM
4+5	HVSGGHVNPAVTFGALIGGRI**S**VIRAVYYWIAQLLGSIVAALVLRLVTNNMRPSGFHVSPGVGVGHM
6	FILEVVM
7	TFGLM
8	YTVYGTAIDPKRGAVSNIAPLAIGLIVGANILVGGPFDGACM
9	NPALAFGPSLVGWQWHQHWIFWVGPLLGAALAALVYEYAVIPIEPPPHHHQPLATEDY
9his	NPALAFGPSLVGWQWHQHWIFWVGPLLGAALAALVYEYAVIPIEPPPHHHQPLATEDYGGGHHHHHH

[a] The expected mass list is presented as the expected average protonated mass. The amino acid sequence of fragments is shown in the bottom section of table, in single-letter amino acid code. Potential phosphoserine residues are boxed in black.

The yield of purified, expressed protein was ~1 mg from 50 g of wet cells, which is an average amount for heterologous membrane proteins produced in *P. pastoris* (*35*). Coomassie-stained gels indicated that Ni^{2+} affinity column-purified PvTIP3;1 was >90% pure (Figure 1a). Yeast cultures grown to high cell density can result in an increased level of proteolysis of expressed protein (*35*); however, Western immunoblotting showed no significant proteolytic degradation of purified PvTIP3;1 (Figure 1b).

Phosphorylation of Overexpressed PvTIP3;1-G_3-H_6. As discussed above, the water channel activity of PvTIP3;1 is activated by phosphorylation (*14*). In vitro phosphorylation by a native, membrane-associated CDPK occurs at an amino-terminal serine, most likely Ser7 (*15*). We used MALDI-TOF MS to test whether recombinant PvTIP3;1-G_3-H_6 was authentically phosphorylated in *P. pastoris*.

Hydrophobic integral membrane proteins can be problematic to study by MS. When using in-gel trypsin or cyanogen bromide digestion techniques (*37*), >3 kDa peptides usually cannot be detected by MS. Our method of preparing PvTIP3;1-G_3-H_6 for MALDI-TOF MS was derived from that of Pawate et al. (*38*). Protein was denatured with detergent, isolated by gel electrophoresis, and then electroblotted to pure nitrocellulose. Nitrocellulose-bound PvTIP3;1-G_3-H_6 was cleaved with cyanogen bromide, and the resulting peptides were recovered by dissolving the paper in acetone or a mixture of acetone and acetonitrile. The solubilized peptides were subsequently analyzed by MALDI-TOF.

Most mass peaks in MALDI-TOF spectra from cyanogen bromide fragments of native PvTIP3;1 and recombinant PvTIP3;1-G_3-H_6 (Figure 2) could be assigned (Table 1) and accounted for ~79% of the amino acid sequence. Mass peaks smaller than *m*/*z* 1200 could not be assigned, and most are likely generated by the various matrix compounds (data not shown).

The peak of CNBr fragment 2 from native PvTIP3;1 (Figure 2a) was shifted by *m*/*z* +42 from the predicted mass, corresponding to a peptide acetylation within amino acids 2−20. This suggests that a fraction of the expressed protein undergoes N-terminal processing, whereby Ala2 is acetylated following removal of the N-terminal residue by methionine aminopeptidase. Acetylated moieties were not observed for any other detected fragment. The major peak of CNBr fragment 2 from *Pichia*-expressed PvTIP3;1-G_3-H_6 was of the expected mass; however, a significant peak was observed at *m*/*z* +42 (Figure 2b), corresponding to a peptide acetylation, which suggested that a fraction of the expressed protein undergoes N-terminal processing as occurs with the native protein.

Minor peaks were seen at positions *m*/*z* +80 to CNBr fragment 2 of both native and recombinant PvTIP3;1, corresponding to a single phosphorylation event (Figure 2a,b). This minor phosphorylation peak was not detected in reflectron mode MALDI-TOF (data not shown), which is characteristic of phosphopeptides, resulting from the physical loss of the phosphate group during ion reflection (*39*).

Table 2: Predicted and Observed Trypsin Fragments of PvTIP3;1[a]

			Observed mass					
			PvTIP3;1-G_3-H_6 expressed in *Pichia pastoris*			Native PvTIP3;1		
			treatment			treatment		
Fragment	Residues	Expected mass	Untreated	λ-PPase	PKA	Untreated	λ-PPase	PKA
1	1-4	478.60	-	-	-	-	-	-
1ptr	2-4	347.39	347.66, +42	347.29, +42	347.50, +42	-	-	-
2	5	156.19	-	-	-	-	-	-
3	6-10	629.70	629.91	629.18	-	-	-	-
2+3	5-10	785.89	786.11, +80	785.16	865.54	785.38, +80	785.38	865.31
4	11-21	1260.3	1261.0	1258.9	1259.5	1259.5	1259.5	1259.5
3+4	6-21	1871.0	-	-	-	1869.7	1869.8	-
2+3+4	5-21	2027.2	-	-	-	2105.8	2025.9	2105.7
5	22-46	2534.0	-	-	-	2533	2532.2	2532.2
6	47-97	5086.9	-	-	-	-	-	-
7	98-102	587.75	587.98	587.23	-	-	-	-
8	103-122	2220.7	-	-	-	2219.2	2219.4	2219.1
9	123-167	4885.8	-	-	-	-	-	-
10	168	156.19	-	-	-	-	-	-
11his	169-265	10311	-	-	-	-	-	-

Fragment	Amino Acids
1	MATR
1ptr	ATR
2	R
3	Y**S**FGR
2+3	RY**S**FGR
4	TDEATHPDSMR
3+4	Y**S**FGRTDEATHPDSMR
2+3+4	RY**S**FGRTDEATHPDSMR
5	A**S**LAEFASTFIFVFAGEGSGLALVK
6	IYQDSAFSAGELLALALAHAFALFAAVSASMHVSGGHVNPAVTFGALIGGR
7	I**S**VIR
8	AVYYWIAQLLGSIVAALVLR
9	LVTNNMRPSGFHVSPGVGVGHMFILEVVMTFGLMYTVYGTAIDPK
10	R
11his	GAVSNIAPLAIGLIVGANILVGGPFDGACMNPALAFGPSLVGWQWHQHWIF WVGPLLGAALAALVYEYAVIPIEPPPHHHQPLATEDYGGGHHHHHH

[a] The expected mass list is presented as the expected average protonated mass. The amino acid sequence of fragments is shown in the bottom section of the table, in single-letter amino acid code. Trypsin cleaves poorly when a phosphoserine residue is the second amino acid following the cleavage site (*40*), which would result in the absence of fragment 3 following PKA treatment. Partial cleavage can result when Arg residues occur in tandem or at the peptide N-terminus (*64*), illustrated by the presence of fragment 2+3. Acidic residues flanking the cleavage site will also inhibit trypsin activity (*64*), which would explain the presence of fragment 2+3+4. Potential phosphoserine residues are boxed in black. Fragment 1ptr results from the post-translational removal of the amino-terminal methionine.

Phosphorylated moieties were not observed for any other detected fragment.

Treatment of expressed PvTIP3;1-G_3-H_6 with λ protein phosphatase (λ-PPase) eliminated the *m*/*z* +80 peak of CNBr fragment 2 and did not significantly change the mass of any other observed fragment (Figure 2c). Conversely, treatment of PvTIP3;1-G_3-H_6 with protein kinase A (PKA) eliminated the parent ion peak and greatly increased the size of the +80 *m*/*z* peak (Figure 2d). In addition, a minor peak at *m*/*z* +122 was seen, corresponding to CNBr fragment 2 that is both acetylated and phosphorylated.

To verify the phosphorylation of Ser7, we performed in-solution trypsin digestion of recombinant PvTIP3;1-G_3-H_6. Generally, only peptides corresponding to the N-terminus were detected by MALDI-TOF MS using this method. The peak of tryptic fragment 2+3 from the recombinant protein was accompanied by a peak at *m*/*z* +80 (Figure 3a), corresponding to a single phosphorylation event. Phosphorylated tryptic fragment 3 was not observed. A similar pattern was observed with trypsin-digested native PvTIP3;1 (Figure 4a). Trypsin cleaves poorly when a phosphoserine or phosphothreonine residue is the second amino acid following the cleavage site (*40*), which explains the absence of the fragment and further supports the evidence of Ser7 phosphorylation in both native and recombinant protein. Peptide 1ptr, corresponding to the N-terminus lacking a Met1 residue, was found in both acetylated (*m*/*z* +42) and nonacetylated forms (Figure 3), confirming that a significant fraction of the recombinant protein undergoes N-terminal processing.

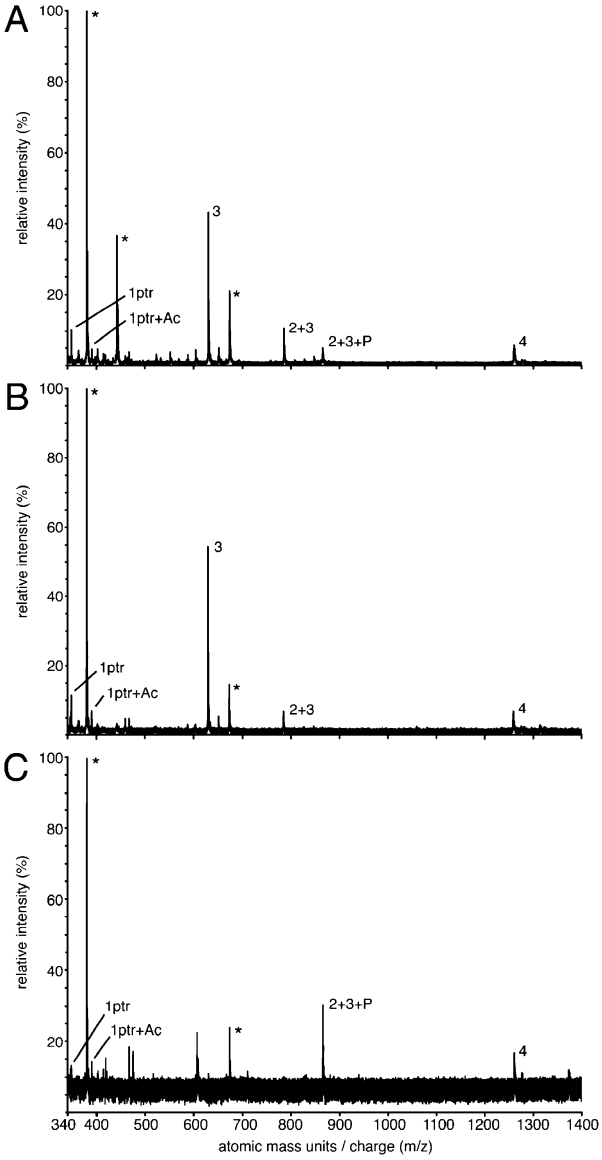

FIGURE 3: Linear MALDI-TOF mass spectra from trypsin digests of PvTIP3;1-G_3-H_6 expressed in *P. pastoris*. Peaks labeled by fragment number as described in Table 2. Ac denotes peptide acetylation, P denotes peptide phosphorylation, and asterisks indicate matrix peaks. (A) Recombinant PvTIP3;1-G_3-H_6. The fragment 1ptr peak is accompanied by a minor peak at m/z +42 (peptide acetylation). The fragment 2+3 peak is followed by a minor peak at m/z +80 (peptide phosphorylation). (B) Recombinant PvTIP3;1-G_3-H_6 treated with λ-PPase. The fragment 1ptr peak is accompanied by a minor peak at m/z +42 (peptide acetylation). The peak of phosphorylated fragment 2+3 is no longer evident, and the intensity of the fragment 3 peak is increased relative to those of the matrix peaks. (C) Recombinant PvTIP3;1-G_3-H_6 treated with PKA. The fragment 1ptr peak is accompanied by a minor peak at m/z +42 (peptide acetylation). Fragment 2+3 and fragment 3 peaks are not present; the major peak is from the phosphorylated peptide m/z +80 from fragment 2+3. Note that peaks of other PvTIP3;1-G_3-H_6 fragments do not experience significant changes in mass with either λ-PPase or PKA treatment, suggesting that no other amino-terminal serine or threonine residues are phosphorylated.

Treatment of recombinant PvTIP3;1-G_3-H_6 with λ-PPase eliminated the m/z +80 peak of tryptic fragment 2+3 and did not significantly change the mass of any other observed fragment (Figure 3b). Additionally, the peak intensity of tryptic fragment 3 increased relative to those of the other

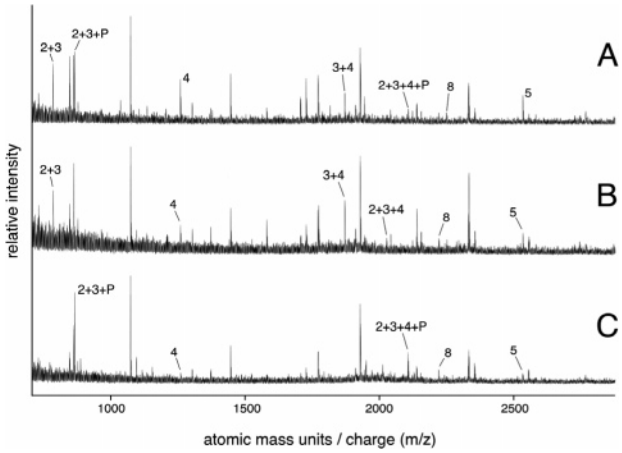

FIGURE 4: Reflectron MALDI-TOF mass spectra from trypsin digests of PvTIP3;1 isolated from *Ph. vulgaris* seed. Peaks labeled by fragment number as described in Table 2. The letter P denotes peptide phosphorylation. Note that trypsin will not cleave when a phosphoserine residue is the second amino acid following the susceptible bond (*40*), or when acidic residues are nearby (*64*). (A) Native PvTIP3;1. The fragment 2+3 peak is accompanied by a peak at m/z +80 (peptide phosphorylation). A minor peak that is m/z +80 greater than the expected mass of fragment 2+3+4 is also observed. (B) Native PvTIP3;1 treated with λ-PPase. The peak of phosphorylated fragment 2+3 is no longer evident, and the peak of unphosphorylated fragment 2+3+4 is evident. (C) Native PvTIP3;1 treated with PKA. The fragment 2+3 and fragment 2+3+4 peaks are not present; peaks corresponding to phosphorylated peptides m/z +80 from fragment 2+3 and fragment 2+3+4 are observed. Delayed extraction of ionized peptides into the spectrometer column prevented the loss of phosphate from the phosphopeptides during ion reflection.

peptide and matrix peaks. Conversely, treatment of PvTIP3;1-G_3-H_6 with PKA eliminated the parent ion peak of either tryptic fragment 3 or fragment 2+3 and greatly increased the m/z +80 peak of tryptic fragment 2+3 (Figure 3c). Similar results were observed with native PvTIP3;1 (Figure 4b,c). λ-PPase or PKA treatment did not change the mass of tryptic fragment 1ptr or 4. Peaks corresponding to trypsin fragment 1 or 1ptr were not observed with native PvTIP3;1.

Molecular Modeling of the PvTIP3;1 Structure. To predict the molecular environment of Ser7, Ser23, and Ser99, we generated molecular models of PvTIP3;1 using the atomic structures of homologous aquaporins as templates. High-resolution, three-dimensional (3D) structures are available for human and bovine AQP1 (*12*, *41*) and ovine AQP0 (*42*). The amino acid sequences of these aquaporins were aligned with that of PvTIP3;1 (Figure 5), and the Modeller software package (*29*) was used to generate 3D models of PvTIP3;1 by homology modeling (Table S1 of the Supporting Information). Since the aquaporin templates used to build the homology model were 35−38% identical to PvTIP3;1, the careful alignment of multiple templates with the target sequence should result in a degree of structural overlap significantly greater than 80% (*43*). Nine amino-terminal residues and two carboxy-terminal residues could not be modeled since the corresponding residues in homologous proteins did not have defined structures (Figure 5). Five models were generated and superimposed (Figure 6). The Modeller objective scoring function and protein stereochemistry showed that the best model had no residues with disallowed ϕ or ψ angles. Compared to the template aquaporin structures, the best model had an α-carbon rms

```
BtAQP1      1 ---------MASEFKKKLFWRAVVAEFLAMILFIFISIGSALGFHYPIKSNQTTGAVQDNVKVSLAFGLSIATLAQSVGH 71
HsAQP1      1 ---------masefkkkLFWRAVVAEFLATTLFVFISIGSALGFKYPVGNNQT--AVQDNVKVSLAFGLSIATLAQSVGH 69
OaAQP0      1 ----------mwelRSASFWRAIFAEFFATLFYVFFGLGASLRWAP---------GPLHVLQVALAFGLALATLVQAVGH 61
PvTIP3;1    1 matrrysfgRTDEATHPDSMRASLAEFASTFIFVFAGEGSGLALVKIYQDSAF--SAGELLALALAHAFALFAAVSASMH 78

BtAQP1     72 ISGAHLNPAVTLGLLLSCQISVLRAIMYIIAQCVGAIVATAILSGITSSLPDNSLGLNALAPGVNSGQGLGIEIIGTLQL 151
HsAQP1     70 ISGAHLNPAVTLGLLLSCQISIFRALMYIIAQCVGAIVATAILSGITSSLTGNSLGRNDLADGVNSGQGLGIEIIGTLQL 149
OaAQP0     62 ISGAHVNPAVTFAFLVGSQMSLLRAICYVVAQLLGAVAGAAVLYSVTPPAVRGNLALNTLHPGVSVGQATIVEIFLTLQF 141
PvTIP3;1   79 VSGGHVNPAVSFGALIGGRISVIRAVYYWIAQLLGSIVAALVLRLVTNNMRPSGF---HVSPGVGVGHMFILEVVMTFGL 155

BtAQP1    152 VLCVLATT-DRRRRDLGGSGPLAIGFSVALGHLLAIDYTGCGINPARSFGSSVITHNFQDHWIFWVGPFIGAALAVLIYD 230
HsAQP1    150 VLCVLATT-DRRRRDLGGSAPLAIGLSVALGHLLAIDYTGCGINPARSFGSAVITHNFSNHWIFWVGPFIGGALAVLIYD 228
OaAQP0    142 VLCIFATY-DERRNGRLGSVALAVGFSLTLGHLFGMYYTGAGMNPARSFAPAILTRNFTNHWVYWVGPVIGAGLGSLLYD 220
PvTIP3;1  156 MYTVYGTAIDPKRGAVSYIAPLAIGLIVGANILVGGPFDGACMNPALAFGPSLVGWQWHQHWIFWVGPLLGAALAALVYE 235

BtAQP1    231 SSVITHNFQDHWIFWVGPFIGAALAVLIYDFILAPRSSDLTDRVKVWTSgqveeydldaddinsrvemkpk-- 271
HsAQP1    229 SAVITHNFSNHWIFWVGPFIGGALAVLIYDFILAPrssdltdrvkvwtsgqveeydldaddinsrvemkpk-- 269
OaAQP0    221 PAILTRNFTNHWVYWVGPVIGAGLGSLLYDFLLFPRLKSVSERLSILKGtrpsesngqpevtgepvelktqal 263
PvTIP3;1  236 PSLVGWQWHQHWIFWVGPLLGAALAALVYEYAVIPIEPPPHHHQPLATEdy---------------------- 256
```

FIGURE 5: Sequence alignment of bovine and human AQP1, ovine AQP0, and PvTIP3;1. Amino acid residues are indicated by the single-letter amino acid code. Uppercase letters are used for residues present in the relevant atomic structure or model, and lowercase letters are used for residues not present in the crystal structures. Cytoplasmic consensus sites of PKA phosphorylation (Ser7, Ser23, and Ser99) in PvTIP3;1 are boxed in black. Transmembrane α-helical residues are shown in boldface type.

deviation of 0.8 Å and a structural diversity of 0.9−1.3 Å.

This analysis showed that Ser23 is located within the transmembrane domain of the first membrane-spanning helix, whereas Ser99 appears to be slightly buried within the protein, beneath the carboxy-terminal domain (Figure 6). Ser7 could not be modeled since there is no corresponding template structure. One should note that electron densities for the amino-terminal domains of ovine AQP0, human AQP1, and the homologous bacterial glycerol channel GlpF are disordered (*10*−*12*, *42*). Such disordered domains have a much higher likelihood of being phosphorylated than structurally ordered regions (*34*). The program DISPHOS, which calculates phosphorylation site probabilities on the basis of position-specific and disorder parameters (*34*), predicts that PvTIP3;1 residues Ser7 and Ser51 are phosphorylated (Table S2 of the Supporting Information). According to our structural model, however, Ser51 is on a loop projecting into the vacuolar lumen and is therefore unlikely to be phosphorylated. These observations, combined with the extramembrane location of the amino terminus, suggest that Ser7 is in a flexible domain exposed to the cytoplasm. Our results therefore indicate that Ser7 is accessible to cytoplasmic kinases, whereas Ser23 and Ser99 would be inaccessible.

DISCUSSION

In this study, we examine the ability of protein kinase A to phosphorylate the plant aquaporin PvTIP3;1 in vitro and mimic the in vivo phosphorylation state. Mass spectrometry showed that PKA phosphorylation only occurred at the amino-terminal residue Ser7, which is identical to the results of previous studies of in vivo phosphorylation. Molecular modeling suggested that this is the only amino-terminal serine accessible to cytoplasmic kinases.

Aquaporins Are Abundant in Plants. Plants possess a surprising variety of aquaporins and other MIP family proteins. To date, more than 100 isoforms have been identified; curiously, 38 have been found in the *A. thaliana* genome, while only 13 have been identified in the human genome. The relative abundance of these proteins in plants is thought to be due to the greater number of selectively filtered compounds and the wider variety of subcellular membrane targets and regulatory mechanisms (*44*, *45*).

As a strict aquaporin, PvTIP3;1 is selective for water and impermeable to ions and small nonpolar solutes such as glycerol and urea (*13*, *14*). The protein accumulates in membranes of protein storage vacuoles during embryo maturation and disappears rapidly after germination (*46*, *47*). PvTIP3;1 may therefore play important roles during embryo desiccation (*48*) and seed germination (*13*). Whether PvTIP3;1 functions primarily during seed development or after germination is unclear. Nevertheless, it is thought to have an important and evolutionarily conserved function since it shares immunogenic epitopes and sequence identity with seed membrane proteins in a wide variety of plant species (*21*, *46*, *49*−*51*).

PvTIP3;1 cDNA expressed in *Xenopus* toad oocytes shows phosphorylation-regulated aquaporin activity (*14*), so the channel appears to be fully functional by itself. However, it is possible that PvTIP3;1 forms heterotetramers with another aquaporin in vivo, as observed by Harvengt et al. (*21*), who detected oligomers of two MIP family proteins in the vacuole membrane of lentil seed. Several aquaporin homologues are found in bean and *A. thaliana* seed (*23*, *49*), but there is no evidence to suggest that PvTIP3;1 participates in the formation of heterotetramers.

Mass Spectrometry Shows that Ser7 Is Phosphorylated. The ability to manipulate the phosphorylation state of recombinant PvTIP3;1-G_3-H_6 will allow generation of both the phosphorylated, open form and the dephosphorylated, closed form of this channel for structural studies. We used cyanogen bromide digestion of nitrocellulose-bound protein and MALDI-TOF MS to identify phosphorylated PvTIP3;1 peptides. Our approach combines a number of techniques that are important for the characterization of large and small peptides from this integral membrane protein. Denaturation was important for efficient proteolysis, while subsequent gel electrophoresis and electroblotting removed detergent that would otherwise interfere with MS. Consequently, the protein was transferred to nitrocellulose prior to proteolysis since the entire substrate−peptide matrix could then be solubilized

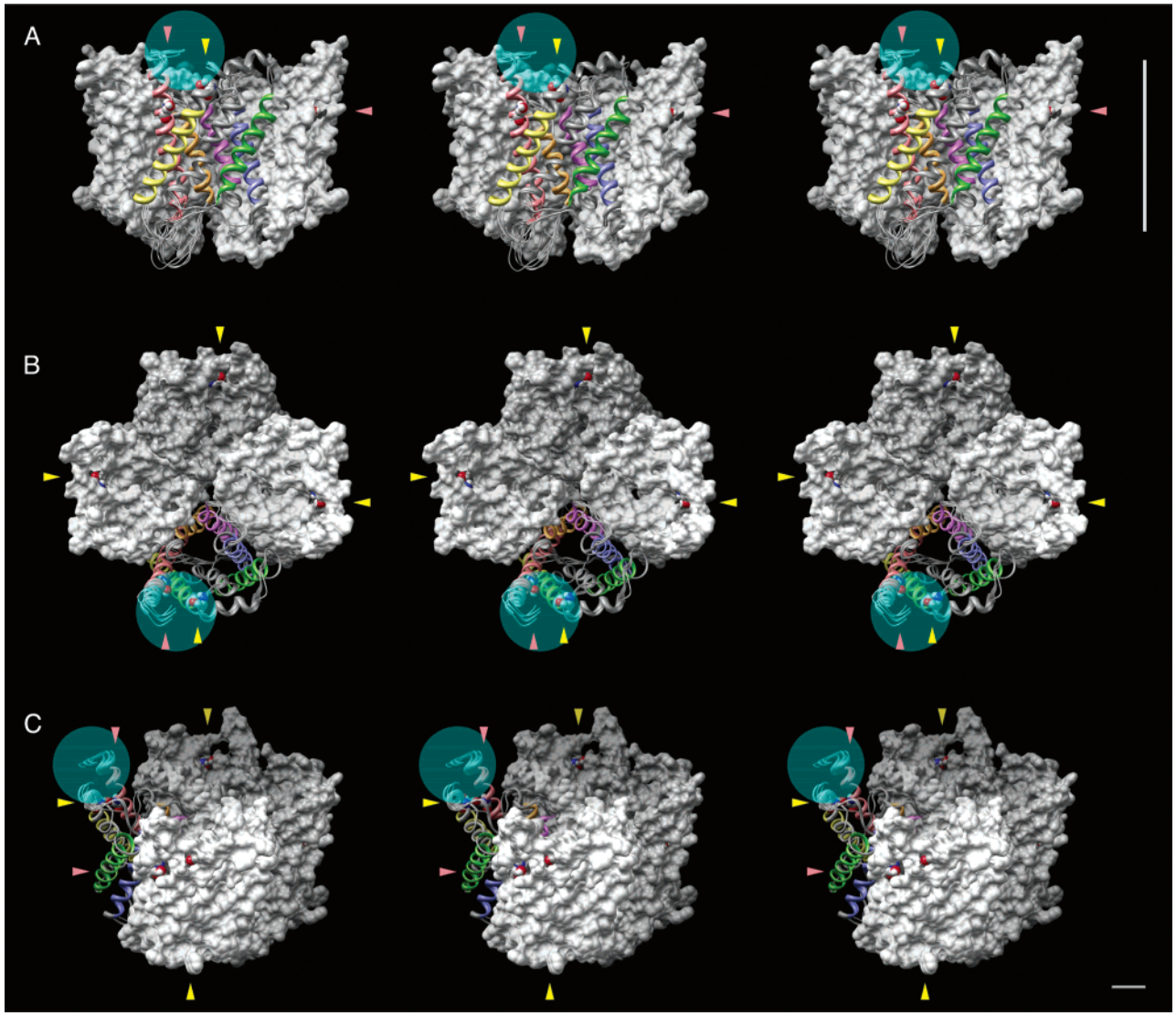

FIGURE 6: Stereo model of PvTIP3;1 aquaporin based on homology modeling with the crystal structures of AQP0 (*42*) and AQP1 (*12*, *41*). The left- and right-hand pairs correspond to wall-eyed and cross-eyed stereoviews. One subunit in the tetramer is shown as a ribbon model, and three subunits are shown as molecular surface models. Ser23 and Ser99 are highlighted with red and yellow arrowheads, respectively, and displayed as spherical atoms. The ribbon model is an overlay of five possible calculated structures. The model with the lowest free energy and best scoring was used to generate the molecular surface. (A) Side view, with cytoplasmic face up and vacuolar face down. The green circle represents the probable boundary for the location of Ser7. The vertical bar denotes 50 Å and the approximate span of the lipid bilayer in relation to the protein tetramer. (B) View of the cytoplasmic face, tilted by 5°. (C) Side view, with the tetramer from panel B rotated by 90° and tilted by 30°. The scale bar is 10 Å.

and subjected to MALDI-TOF MS. Trypsin digestion and MALDI-TOF MS of gel-bound, native PvTIP3;1 and solubilized, recombinant PvTIP3;1-G_3-H_6 were used to confirm that the phosphorylation of Ser7 observed in vivo was identical to that generated in vitro by PKA.

Previous studies have shown that PvTIP3;1 is phosphorylated in vivo by a membrane-bound CDPK at an amino-terminal serine (*15*). Potential sites for CDPK phosphorylation include Ser7, Ser23, and Ser99, which have been implicated in channel regulation (*14*, *15*). Partial phosphorylation of both native PvTIP3;1 and recombinant PvTIP3;1-G_3-H_6 was detected by MALDI-TOF MS (Figures 2a,b, 3a, and 4a). MS showed that phosphorylation was observed in only CNBr fragment 2, where Ser7 lies within the only CDPK motif of this amino-terminal peptide (*52*, *53*). No phosphorylation-associated mass was observed in CNBr fragments 3 and 4, which contain residues Ser23 and Ser99. Phage λ protein phosphatase was able to completely dephosphorylate Ser7 (Figures 2c, 3b, and 4b). Protein kinase A (PKA) is one of the most thoroughly studied protein kinases, and its phosphorylation site specificities have been well characterized (*54*, *55*). The consensus sequence for PKA phosphorylation is Arg-Arg-X-Ser/Thr-B, where B represents a large hydrophobic residue. Ser7 lies within a model consensus sequence Arg-Arg-Tyr-Ser-Phe, whereas Ser23 and Ser99 lie within the poor PKA motif Arg-X-Ser. No other Ser or Thr residues of PvTIP3;1 lie within possible PKA phosphorylation sites. Consequently, PKA was used to phosphorylate Ser7 in vitro, and complete conversion of unphosphorylated to phosphorylated protein was achieved (Figures 2d, 3c, and 4c). However, even the promiscuous kinase activity of PKA could not produce detectable phosphorylation of Ser23 and Ser99 (Figure 2d). In addition, a tryptic fragment corresponding to amino acids 6−10 was

the only peptide of the N-terminus affected by PKA treatment (Figures 3c and 4c), supporting the idea that Ser7 is the only site of phosphorylation.

Curiously, native and recombinant PvTIP3;1 CNBr fragment 2 appears m/z +42 higher than its expected position, indicating that the peptide is acetylated. Previous mass spectrometry of the native protein had not discovered any such modification (*15*). The amino-terminal Met-Ala-Thr sequence of PvTIP3;1 is a likely target of methionine aminopeptidase and amino-terminal acetyltransferases (*56*). Acetylation does not appear to affect phosphorylation of PvTIP3;1-G_3-H_6 since phosphopeptides corresponding to both unprocessed and acetylated CNBr fragment 2 are observed following treatment by PKA (Figure 2d). Amino-terminal acetylation can have various effects on protein stability, activity, and interprotein interactions (*56*), so the role of PvTIP3;1 acetylation is unclear.

Molecular Modeling Showed that Ser23 and Ser99 Are Inaccessible for Phosphorylation. To correlate our results with the protein structure, we generated models of PvTIP3;1 by homology modeling using templates based on the atomic-resolution structures of bovine and human AQP1 (*12*, *41*) and ovine AQP0 (*42*). Our model shows that Ser23 is buried within the lipid bilayer on transmembrane helix 1, and that Ser99 is located at the amino-terminal end of transmembrane helix 3 on the turn following the first NPA motif hemihelix (Figure 6). It is possible for this latter residue to be exposed to the cytoplasm if the carboxy-terminal domain were to move; however, it is in such a buried location of the cytoplasmic face that it would be unlikely to interact with a kinase. The disordered electron density of the amino-terminal domains of AQP1 and GlpF indicates significant conformational flexibility that would facilitate the accessibility of kinases and is a feature characterized by an enhanced likelihood of phosphorylation (*34*).

Although mutations of Ser23 and Ser99 in PvTIP3;1 affect water channel activity, our results suggest that they cannot be phosphorylated. It is possible that these residues interact with phosphorylated Ser7, or that they are sufficiently close to phosphorylated Ser7 that mutations may affect the orientation or charge of adjacent residues that interact with the phosphate.

Phosphorylation Is a Widely Used Mechanism for Gating Plant Aquaporins. Phosphorylation is also known to enhance aquaporin activity in the plant aquaporins SoPIP2;1 and GmNod26. SoPIP2;1 is phosphorylated in vivo at the carboxy terminus on Ser274 via a membrane-associated CDPK (*16*). Mutational analysis demonstrated that both Ser274 and Ser115 affect channel regulation, but phosphorylation of Ser115 was not observed (*17*). Possible explanations for this effect include the lack of activity from an appropriate kinase or the rapid loss of phosphate. GmNod26 is similarly phosphorylated in vivo by a membrane-associated CDPK, at the carboxy terminus on Ser262 (*20*). In addition, phosphorylation of several *Arabidopsis* and tulip plasma membrane aquaporins (*57*, *58*) has been detected, suggesting that this modification may be common among plant aquaporins.

Phosphorylation of plant aquaporins PvTIP3;1, SoPIP2;1, and GmNod26 occurs on the protein termini, which one can predict to be fairly mobile given that these domains are disordered in the aquaporin crystal structures (*11*, *12*, *42*). Consequently, there may be a common mechanism for channel gating, possibly due to physical occlusion of the pore by the unphosphorylated amino- or carboxy-terminal domain. The amino terminus of PvTIP3;1 and the carboxy termini of SoPIP2;1 and GmNod26 have an overall basic character. Positively charged residues in these domains could interact electrostatically with acidic residues around the pore vestibule and favor a closed state in which the water channel is blocked. In such a case, the addition of a negatively charged phosphate group would disrupt this interaction and open the channel. The observation that SoPIP2;1 and GmNod26 phosphorylation null mutants have a constitutively low activity (*17*, *20*) supports this hypothesis. An alternative mechanism of aquaporin gating has recently been proposed, in which the charge of histidine residues in extracellular loops can organize water molecules within the pore vestibule and thereby restrict the flow of water through the channel in a pH-dependent manner (*59*). A charged phosphate on Ser7 of PvTIP3;1 could have an analogous effect, but the flexibility of the amino terminus would abrogate any effect on the ordering of water molecules.

Dehydration-induced CDPKs have been found in *Arabidopsis* (*60*), spinach (*16*), and *Mesembryanthemum* (*61*); similar kinases may exist in *Phaseolus*. Our hypothesis is that unphosphorylated PvTIP3;1 channels are in a closed conformation early in embryo development to keep the rate of seed dehydration optimally low. Immediately prior to embryo dormancy, PvTIP3;1 is phosphorylated by dehydration-induced CDPK(s) and the channels open, thereby priming the seed for water uptake upon germination.

Regulation of channel function by protein phosphorylation is a mechanism common in both plant and animal systems. For instance, CDPK phosphorylation of the cystic fibrosis transmembrane conductance regulator channels, L-type Ca^{2+} channels, and Ca^{2+}-dependent K^+ channels is necessary either for channel opening or for increasing the size of the channel open state (*62*, *63*). Obviously, we have a limited understanding of the structural rearrangements that underlie phosphorylation-dependent channel regulation, despite the abundance and importance of transmembrane proteins. Characterization of phosphorylation-mediated gating in PvTIP3;1 will serve as a paradigm for understanding gating mechanisms of other channels.

ACKNOWLEDGMENT

We are grateful to Daniel Schweissinger for excellent technical assistance. We thank Jane Wu for performing the trypsin digestion of PvTIP3;1 and subsequent MALDI-TOF reflectron mass spectrometry shown in Figure 4. We are grateful to Vijay Reddy, Christopher Roth, Larry Brill, and Bill Webb for helpful suggestions and discussions and to François Chaumont for critical reading of the manuscript.

SUPPORTING INFORMATION AVAILABLE

Evaluation of PvTIP3;1 model structures (Table S1), disorder and position-based prediction of TIP3;1 phosphorylation sites (Table S2), and Protein Data Bank coordinates. This material is available free of charge via the Internet at http://pubs.acs.org.

REFERENCES

1. Preston, G. M., and Agre, P. (1991) Isolation of the cDNA for erythrocyte integral membrane protein of 28 kilodaltons: Member

of an ancient channel family, *Proc. Natl. Acad. Sci. U.S.A. 88*, 11110−11114.
2. Preston, G. M., Carroll, T. P., Guggino, W. B., and Agre, P. (1992) Appearance of water channels in *Xenopus* oocytes expressing red cell CHIP28 protein, *Science 256*, 385−387.
3. Pao, G. M., Wu, L. F., Johnson, K. D., Höfte, H., Chrispeels, M. J., Sweet, G., Sandal, N. N., and Saier, M. H. (1991) Evolution of the MIP family of integral membrane transport proteins, *Mol. Microbiol. 5*, 33−37.
4. Chepelinsky, A. (1994) in *Handbook of Membrane Channels: Molecular and Cellular Physiology* (Perrachia, C., Ed.) pp 413−432, Academic Press, San Diego.
5. Le Cahérec, F., Deschamps, S., Delamarche, C., Pellerin, I., Bonnec, G., Guillam, M. T., Thomas, D., Gouranton, J., and Hubert, J. F. (1996) Molecular cloning and characterization of an insect aquaporin: Functional comparison with aquaporin 1, *Eur. J. Biochem. 241*, 707−715.
6. Park, J. H., and Saier, M. H. (1996) Phylogenetic characterization of the MIP family of transmembrane channel proteins, *J. Membr. Biol. 153*, 171−180.
7. Agre, P., Sasaki, S., and Chrispeels, M. J. (1993) Aquaporins: A family of water channel proteins, *Am. J. Physiol. 265*, F461.
8. Chrispeels, M. J., and Agre, P. (1994) Aquaporins: Water channel proteins of plant and animal cells, *Trends Biochem. Sci. 19*, 421−425.
9. Maurel, C. (1997) Aquaporins and water permeability of plant membranes, *Annu. Rev. Plant Physiol. Plant Mol. Biol. 48*, 399−429.
10. Fu, D., Libson, A., Miercke, L. J. W., Weitzman, C., Nollert, P., Krucinski, J., and Stroud, R. M. (2000) Structure of a glycerol-conducting channel and the basis for its selectivity, *Science 290*, 481−486.
11. Murata, K., Mitsuoka, K., Hirai, T., Walz, T., Agre, P., Heymann, J. B., Engel, A., and Fujiyoshi, Y. (2000) Structural determinants of water permeation through aquaporin-1, *Nature 407*, 599−605.
12. Sui, H., Han, B.-G., Lee, J. K., Walian, P., and Jap, B. K. (2001) Structural basis of water-specific transport through the AQP1 water channel, *Nature 414*, 872−877.
13. Maurel, C., Chrispeels, M., Lurin, C., Tacnet, F., Geelen, D., Ripoche, P., and Guern, J. (1997) Function and regulation of seed aquaporins, *J. Exp. Bot. 48*, 421−430.
14. Maurel, C., Kado, R. T., Guern, J., and Chrispeels, M. J. (1995) Phosphorylation regulates the water channel activity of the seed-specific aquaporin α-TIP, *EMBO J. 14*, 3028−3035.
15. Johnson, K. D., and Chrispeels, M. J. (1992) Tonoplast-bound protein kinase phosphorylates tonoplast intrinsic protein, *Plant Physiol. 100*, 1787−1795.
16. Johansson, I., Larsson, C., Ek, B., and Kjellbom, P. (1996) The major integral proteins of spinach leaf plasma membranes are putative aquaporins and are phosphorylated in response to Ca^{2+} and apoplastic water potential, *Plant Cell 8*, 1181−1191.
17. Johansson, I., Karlsson, M., Shukla, V. K., Chrispeels, M. J., Larsson, C., and Kjellbom, P. (1998) Water transport activity of the plasma membrane aquaporin PM28A is regulated by phosphorylation, *Plant Cell 10*, 451−459.
18. Johansson, I., Karlsson, M., Johanson, U., Larsson, C., and Kjellbom, P. (2000) The role of aquaporins in cellular and whole plant water balance, *Biochim. Biophys. Acta 1465*, 324−342.
19. Lee, J. W., Zhang, Y., Weaver, C. D., Shomer, N. H., Louis, C. F., and Roberts, D. M. (1995) Phosphorylation of nodulin 26 on serine 262 affects its voltage-sensitive channel activity in planar lipid bilayers, *J. Biol. Chem. 270*, 27051−27057.
20. Guenther, J. F., Chanmanivone, N., Galetovic, M. P., Wallace, I. S., Cobb, J. A., and Roberts, D. M. (2003) Phosphorylation of soybean nodulin 26 on serine 262 enhances water permeability and is regulated developmentally and by osmotic signals, *Plant Cell 15*, 981−991.
21. Harvengt, P., Vlerick, A., Fuks, B., Wattiez, R., Ruysschaert, J.-M., and Homble, F. (2000) Lentil seed aquaporins form a hetero-oligomer which is phosphorylated by a Mg^{2+}-dependent and Ca^{2+}-regulated kinase, *Biochem. J. 352*, 183−190.
22. Verkman, A. S., and Mitra, A. K. (2000) Structure and function of aquaporin water channels, *Am. J. Physiol. Renal Physiol. 278*, F13−F28.
23. Johnson, K. D., Höfte, H., and Chrispeels, M. J. (1990) An intrinsic tonoplast protein of protein storage vacuoles in seeds is structurally related to a bacterial solute transporter (GlpF), *Plant Cell 2*, 525−532.
24. Merkl, R. (2003) A survey of codon and amino acid frequency bias in microbial genomes focusing on translational efficiency, *J. Mol. Evol. 57*, 453−466.
25. Jahn, T., Dietrich, J., Andersen, B., Leidvik, B., Otter, C., Briving, C., Kühlbrandt, W., and Palmgren, M. G. (2001) Large scale expression, purification and 2D crystallization of recombinant plant plasma membrane H^+-ATPase, *J. Mol. Biol. 309*, 465−476.
26. Daniels, M. J., Chrispeels, M. J., and Yeager, M. (1999) Projection structure of a plant vacuole membrane aquaporin by electron cryo-crystallography, *J. Mol. Biol. 294*, 1337−1349.
27. Hellman, U., Wernstedt, C., Gòñez, J., and Heldin, C.-H. (1995) Improvement of an "in-gel" digestion procedure for the micropreparation of internal protein fragments for amino acid sequencing, *Anal. Biochem. 224*, 451−455.
28. Notredame, C., Higgins, D. G., and Heringa, J. (2000) T-Coffee: A novel method for fast and accurate multiple sequence alignment, *J. Mol. Biol. 302*, 205−217.
29. Fiser, A., and Šali, A. (2003) MODELLER: Generation and refinement of homology-based protein structure models, *Methods Enzymol. 374*, 461−491.
30. Brünger, A. T., Adams, P. D., Clore, G. M., DeLano, W. L., Gros, P., Grosse-Kunstleve, R. W., Jiang, J. S., Kuszewski, J., Nilges, M., Pannu, N. S., Read, R. J., Rice, L. M., Simonson, T., and Warren, G. L. (1998) Crystallography & NMR system: A new software suite for macromolecular structure determination, *Acta Crystallogr. D54* (Part 5), 905−921.
31. Laskowski, R. A., MacArthur, M. W., Moss, D. S., and Thornton, J. M. (1993) PROCHECK: A program to check the stereochemical quality of protein structures, *J. Appl. Crystallogr. 26*, 283−291.
32. Collaborative Computational Project, No. 4 (1994) The CCP4 suite: Programs for protein crystallography, *Acta Crystallogr. D50*, 760−763.
33. Huang, C. C., Couch, G. S., Pettersen, E. F., and Ferrin, T. E. (1996) Chimera: An extensible molecular modeling application constructed using standard components, *Pac. Symp. Biocomput. 1*, 724.
34. Iakoucheva, L. M., Radivojac, P., Brown, C. J., O'Connor, T. R., Sikes, J. G., Obradovic, Z., and Dunker, A. K. (2004) The importance of intrinsic disorder for protein phosphorylation, *Nucleic Acids Res. 32*, 1037−1049.
35. Cregg, J. M., Cereghino, J. L., Shi, J., and Higgins, D. R. (2000) Recombinant protein expression in *Pichia pastoris*, *Mol. Biotechnol. 16*, 23−52.
36. Invitrogen (2000) *Pichia Expression Kit: A Manual of Methods for Expression of Recombinant Proteins in Pichia pastoris*, Invitrogen, Carlsbad, CA.
37. van Montfort, B. A., Canas, B., Duurkens, R., Godovac-Zimmermann, J., and Robillard, G. T. (2002) Improved in-gel approaches to generate peptide maps of integral membrane proteins with matrix-assisted laser desorption/ionization time-of-flight mass spectrometry, *J. Mass Spectrom. 37*, 322−330.
38. Pawate, S., Schey, K. L., Meier, G. P., Ullian, M. E., Mais, D. E., and Halushka, P. V. (1998) Expression, characterization, and purification of C-terminally hexahistidine-tagged thromboxane A_2 receptors, *J. Biol. Chem. 273*, 22753−22760.
39. Annan, R. S., and Carr, S. A. (1996) Phosphopeptide analysis by matrix-assisted laser desorption time-of-flight mass spectrometry, *Anal. Chem. 68*, 3413−3421.
40. Boyle, W. J., van der Geer, P., and Hunter, T. (1991) Phosphopeptide mapping and phosphoamino acid analysis by two-dimensional separation on thin-layer cellulose plates, *Methods Enzymol. 201*, 110−149.
41. de Groot, B. L., Engel, A., and Grubmüller, H. (2001) A refined structure of human aquaporin-1, *FEBS Lett. 504*, 206−211.
42. Gonen, T., Sliz, P., Kistler, J., Cheng, Y., and Walz, T. (2004) Aquaporin-0 membrane junctions reveal the structure of a closed water pore, *Nature 429*, 193−197.
43. Martí-Renom, M. A., Stuart, A. C., Fiser, A., Sánchez, R., Melo, F., and Šali, A. (2000) Comparative protein structure modeling of genes and genomes, *Annu. Rev. Biophys. Biomol. Struct. 29*, 291−325.
44. Santoni, V., Gerbeau, P., Javot, H., and Maurel, C. (2000) The high diversity of aquaporins reveals novel facets of plant membrane functions, *Curr. Opin. Plant Biol. 3*, 476−481.
45. Quigley, F., Rosenberg, J. M., Shachar-Hill, Y., and Bohnert, H. J. (2001) From genome to function: The *Arabidopsis* aquaporins, *Genome Biol. 3*, 1−17.

46. Johnson, K. D., Herman, E. M., and Chrispeels, M. J. (1989) An abundant, highly conserved tonoplast protein in seeds, *Plant Physiol. 91*, 1006−1013.
47. Melroy, D. L., and Herman, E. M. (1991) TIP, an integral membrane protein of the protein-storage vacuoles of the soybean cotyledon undergoes developmentally regulated membrane accumulation and removal, *Planta 184*, 113−122.
48. Robinson, D. G., and Hinz, G. (1997) Vacuole biogenesis and protein transport to the plant vacuole: A comparison with the yeast vacuole and the mammalian lysosome, *Protoplasma 197*, 1−25.
49. Höfte, H., Hubbard, L., Reizer, J., Ludevid, D., Herman, E. M., and Chrispeels, M. J. (1992) Vegetative and seed-specific forms of tonoplast intrinsic protein in the vacuolar membrane of *Arabidopsis thaliana*, *Plant Physiol. 99*, 561−570.
50. Inoue, K., Takeuchi, Y., Nishimura, M., and Hara-Nishimura, I. (1995) Characterization of two integral membrane proteins located in the protein bodies of pumpkin seeds, *Plant Mol. Biol. 28*, 1089−1101.
51. Oliviusson, P., and Hakman, I. (1995) A tonoplast intrinsic protein (TIP) is present in seeds, roots, and somatic embryos of Norway spruce (*Picea abies*), *Physiol. Plant. 95*, 288−295.
52. Johnson, L. N., and Barford, D. (1993) The effects of phosphorylation on the structure and function of proteins, *Annu. Rev. Biophys. Biomol. Struct. 22*, 199−232.
53. Huang, J. Z., Hardin, S. C., and Huber, S. C. (2001) Identification of a novel phosphorylation motif for CDPKs: Phosphorylation of synthetic peptides lacking basic residues at P-3/P-4, *Arch. Biochem. Biophys. 393*, 61−66.
54. Kennelly, P. J., and Krebs, E. G. (1991) Consensus sequences as substrate specificity determinants for protein kinases and protein phosphatases, *J. Biol. Chem. 266*, 15555−15558.
55. Pinna, L. A., and Ruzzene, M. (1996) How do protein kinases recognize their substrates? *Biochim. Biophys. Acta 1314*, 191−225.
56. Polevoda, B., and Sherman, F. (2003) N-Terminal acetyltransferases and sequence requirements for N-terminal acetylation of eukaryotic proteins, *J. Mol. Biol. 325*, 595−622.
57. Santoni, V., Vinh, J., Pflieger, D., Sommerer, N., and Maurel, C. (2003) A proteomic study reveals novel insights into the diversity of aquaporin forms expressed in the plasma membrane of plant roots, *Biochem. J. 373*, 289−296.
58. Azad, A. K., Sawa, Y., Ishikawa, T., and Shibata, H. (2004) Phosphorylation of plasma membrane aquaporin regulates temperature-dependent opening of tulip petals, *Plant Cell Physiol. 45*, 608−617.
59. Németh-Cahalan, K. L., Kalman, K., and Hall, J. E. (2004) Molecular basis of pH and Ca^{2+} regulation of aquaporin water permeability, *J. Gen. Physiol. 123*, 573−580.
60. Urao, T., Katagiri, T., Mizoguchi, T., Yamaguchi-Shinozaki, K., Hayashida, N., and Shinozaki, K. (1994) Two genes that encode Ca^{2+}-dependent protein kinases are induced by drought and high-salt stresses in *Arabidopsis thaliana*, *Mol. Gen. Genet. 244*, 331−340.
61. Chehab, E. W., Patharkar, O. R., Hegeman, A. D., Taybi, T., and Cushman, J. C. (2004) Autophosphorylation and subcellular localization dynamics of a salt- and water deficit-induced calcium-dependent protein kinase from ice plant, *Plant Physiol. 135*, 1430−1446.
62. Gray, P. C., Scott, J. D., and Catterall, W. A. (1998) Regulation of ion channels by cAMP-dependent protein kinase and A-kinase anchoring proteins, *Curr. Opin. Neurobiol. 8*, 330−334.
63. Gadsby, D. C., and Nairn, A. C. (1999) Regulation of CFTR Cl^- ion channels by phosphorylation and dephosphorylation, *Adv. Second Messenger Phosphoprotein Res. 33*, 79−106.
64. Wilkinson, J. M. (1986) in *Practical Protein Chemistry: A Handbook* (Darbre, A., Ed.) pp 121−148, John Wiley and Sons, Chichester, Great Britain.

BI050565D